ARL-TR-8657 • MAR 2019

DEVCOM ARMY RESEARCH LABORATORY

Laser Flash Sintering for Additive Manufacturing of Ceramics

by Deborah Hagen, Desiderio Kovar, Joseph Beaman, and Michael Gammage

NOTICES

Disclaimers

The findings in this report are not to be construed as an official Department of the Army position unless so designated by other authorized documents.

Citation of manufacturer's or trade names does not constitute an official endorsement or approval of the use thereof.

Destroy this report when it is no longer needed. Do not return it to the originator.

ARL-TR-8657 ● MAR 2019

Laser Flash Sintering for Additive Manufacturing of Ceramics

by Deborah Hagen, Desiderio Kovar, and Joseph Beaman
The University of Texas at Austin

Michael Gammage
Weapons and Materials Research Directorate, CCDC Army Research Laboratory

REPORT DOCUMENTATION PAGE

Form Approved
OMB No. 0704-0188

1. REPORT DATE *(DD-MM-YYYY)*	2. REPORT TYPE	3. DATES COVERED (From - To)
March 2019	Technical Report	1 January–31 May 2018

4. TITLE AND SUBTITLE
Laser Flash Sintering for Additive Manufacturing of Ceramics

5a. CONTRACT NUMBER

5b. GRANT NUMBER

5c. PROGRAM ELEMENT NUMBER

6. AUTHOR(S)
Deborah Hagen, Desiderio Kovar, Joseph Beaman, and Michael Gammage

5d. PROJECT NUMBER

5e. TASK NUMBER

5f. WORK UNIT NUMBER

7. PERFORMING ORGANIZATION NAME(S) AND ADDRESS(ES)
US Army Combat Capabilities Development Command, Army Research Laboratory
ATTN: FCDD-RLW-MD
Austin, TX 78758

8. PERFORMING ORGANIZATION REPORT NUMBER
ARL-TR-8657

9. SPONSORING/MONITORING AGENCY NAME(S) AND ADDRESS(ES)

10. SPONSOR/MONITOR'S ACRONYM(S)

11. SPONSOR/MONITOR'S REPORT NUMBER(S)

12. DISTRIBUTION/AVAILABILITY STATEMENT
Approved for public release; distribution is unlimited.

13. SUPPLEMENTARY NOTES

14. ABSTRACT
Additive manufacturing is a promising technology for near-battlefield repair and replacement. The ability to process multiple materials expands the scope of applications. The nScrypt equipment is a multi-material additive manufacturing system designed to dispense inks in a wide range of viscosities. The purpose of this work is to evaluate the feasibility of using laser flash sintering of ceramics using the nScrypt equipment. Laser flash sintering is a novel process that applies an electric field in combination with laser heating of ceramic powder to fuse the ceramic into a solid body. A ceramic slurry containing ceramic powder, solvent, dispersant, and a plasticizer was formulated and dispensed in multiple layers using the nScrypt's pneumatic dispense system. The yttrium aluminum garnet laser in combination with the electric field was used to laser sinter the layers of ceramic. Although laser sintering proved to be very challenging using this system, multilayer ceramic parts were made to full density using a postprocess furnace firing.

15. SUBJECT TERMS
laser flash sintering, direct-write, ceramics, additive manufacturing, suspensions, inks

16. SECURITY CLASSIFICATION OF:			17. LIMITATION OF ABSTRACT	18. NUMBER OF PAGES	19a. NAME OF RESPONSIBLE PERSON
a. REPORT	b. ABSTRACT	c. THIS PAGE			Michael Gammage
Unclassified	Unclassified	Unclassified	UU	48	19b. TELEPHONE NUMBER (Include area code) (512) 232-2696

Contents

List of Figures

List of Tables

1. Introduction

Additive manufacturing (AM) is a powerful manufacturing technique particularly useful for rapid production of customized products able to be produced in small quantities without the typical time and expense of tooling and fixturing. Its promise for near-battlefield supply of needed spare parts and customization of a variety of essentials such as tooling, prosthetics, and custom armor has attracted the attention of the US Army.

Production volumes of polymer and metal parts manufactured with AM have ramped significantly over the past decade. To fully utilize the technology, the use of multiple types of materials and of mixed materials within a product is anticipated. These processes are not yet developed and require additional research. AM of ceramic materials is a prime example because although ceramics excel due to their unique properties in areas such as electronic, sensors, high-temperature materials, corrosion resistance, and lightweight strength, ceramic materials are difficult to process even with conventional means. They are even more difficult to process with AM. The University of Texas is conducting ongoing research in the production of ceramics using innovative AM techniques.

The US Army Research Laboratory (ARL)* South (University of Texas, Austin [UT Austin]) has acquired an n-Scrypt AM machine with multiple dispensing technologies and multiple curing or fusion technologies. This allows potential for evaluating unique multimaterial AM research and development (R&D). The n-Scrypt is capable of dispensing patterned layers using slurries through a narrow stationary nozzle. The dispensing can be patterned by moving the sample with a high-precision x/y table located beneath the nozzle. Alternatively, the n-Scrypt can extrude thermoplastic polymer through a high-temperature nozzle for 3-D printing. The machine is equipped with a yttrium aluminum garnet (YAG) laser with a wavelength of 1 μm, as well as a UV cure lamp for photopolymers and a heated stage. Pick and place capability is also available for placing chips and components.

UT Austin has demonstrated feasibility of direct fusion of zirconium dioxide (zirconia) ceramic using the energy of a carbon dioxide laser with a wavelength of 10.6 μm and application of layers using a ceramic/polymer slurry and a doctor blade. The process, called laser flash sintering, combines the energy of an electric field with lasing to fuse ceramic together. The n-Scrypt was designed to dispense

* As of February 2019, the US Army Research Laboratory has been renamed the US Army Combat Capabilities Development Command - Army Research Laboratory (CCDC-ARL).

slurries of a wide range of viscosities, and it is equipped with a laser that can be rastered with the x/y table to selectively sinter a dispensed slurry. The purpose of this study is to determine if it is feasible to use the n-Scrypt to process ceramics with laser flash sintering.

2. Traditional Ceramic Sintering Overview

Understanding conventional sintering and the mechanism of sintering is instructive to understanding the challenges and the mechanisms of laser sintering. The ultimate goal in sintering is to eliminate the most porosity possible without suffering from excessive grain growth, which may negatively impact physical properties of the ceramic. The thermodynamic driving force for sintering is a reduction in total surface energy. During sintering, atoms move by diffusion (along the surface of particles, through the bulk matrix of crystals, or along grain boundaries) and evaporation/condensation. The direction of mass movement is away from areas of high surface energy toward areas of lower surface energy. The highest energy surface is the air-to-ceramic surface. A grain boundary interface is much lower in energy. Reducing grain boundary area by transferring mass from small grains to larger grains reduces the free energy of the ceramic system even more.

Traditional ceramic sintering is typically divided into three stages, as illustrated Fig. 1. In initial stage sintering, the individual ceramic powder particles fuse together to form small "necks" between particles, but the total density of the ceramic body does not significantly change. Intermediate sintering is characterized by a reduction in surface area and density in the ceramic body, which occurs when porosity is significantly reduced. Final stage sintering starts when remaining porosity is closed off rather than being interconnected. During final stage sintering the porosity is ideally eliminated.

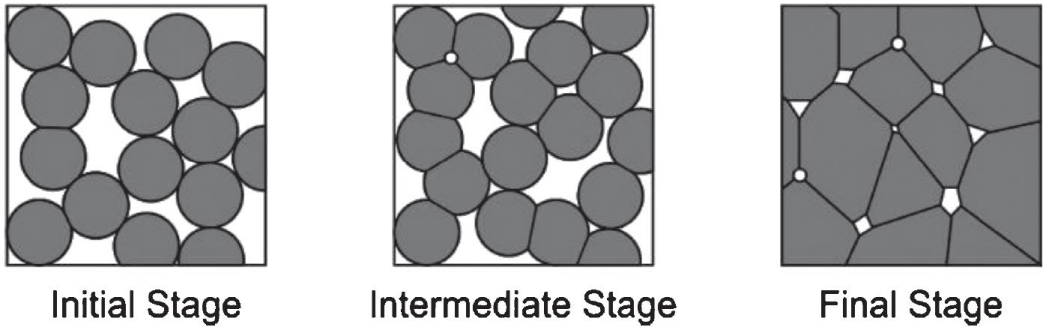

Fig. 1 Stages of ceramics sintering; idealized circular ceramic particles and their changes through the three stages

Initially, particles that touch one another fuse together by replacing two ceramic-to-air interfaces with a single grain-boundary interface, which is much lower in energy. That new grain boundary between touching ceramic particles forms a solid bridge, or neck, between adjacent particles. Neck formation is illustrated in Fig. 2. The particle radius, a, remains constant in this regime, and the neck radius, X, increases by either nondensifying mass transport mechanisms, such as surface diffusion or evaporation condensation, or via densifying mass transport mechanisms such as lattice or grain boundary diffusion, depending on which mechanism is dominant at the temperatures of interest. For the temperatures and materials considered here, surface diffusion is likely the dominant mass transport mechanism in the early stages of sintering, although evaporation/condensation may also play a role, particularly during flash sintering. In either case, neck growth occurs with no significant change in density for these nondensifying mass transport mechanisms. The dominant mechanism for the mass transport required to form necks in initial stage sintering is surface diffusion, meaning that the majority of atoms diffuse along the surface of the particles rather than through the bulk crystal matrix. At high temperatures, vaporization and condensation can also occur in initial stage sintering, although it is rarely the predominant mechanism.

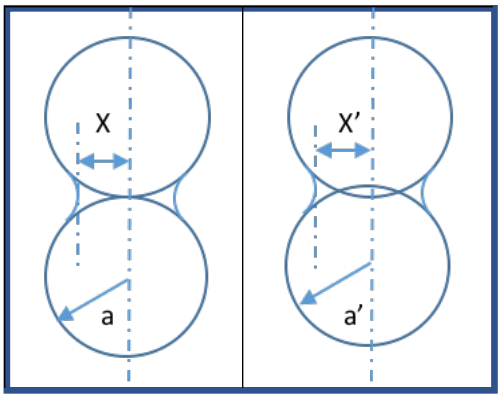

Fig. 2 Two-particle geometric model showing the growth of a neck with radius X for nondensifying initial stage sintering (left) and densifying intermediate stage sintering (right) mass transport mechanisms

Initial stage sintering is the stage on which we are focused for laser flash sintering. The formation of strong necks can form the shape of the part without the strain of layerwise shrinkage. Thermal shock stress will still exist, but since initial stage sintering can occur at lower temperatures than the intermediate and final stages of sintering, thermal shock stress can also be lower than the stress for full densification of the ceramic part under the laser.

3. Ceramic AM Challenges and Direct vs. Indirect Sintering

AM was initially developed for producing parts from polymers. Metal parts are also now routinely produced via direct AM routes by melt processes. However, direct additive routes that do not use a fugitive polymer binder for producing ceramic parts have proven more challenging, and instead the focus has primarily been on indirect methods, including stereolithography, selective laser sintering, ink-jet powder binding, and direct printing (i.e., robocasting). Each of these methods uses a binder to fuse ceramic powder particles together and create a solid part. The binder is subsequently removed by pyrolysis before the parts are sintered to high density. A significant challenge with all of the existing indirect routes is that the presence of the binder limits the sizes of ceramic parts that can be produced because the kinetics of pyrolysis scales with at least the square of the part thickness. If pyrolysis occurs too quickly, gasses released during pyrolysis cannot escape from the interior of the part quickly enough, resulting in cracks or bubble defects. As a result, very long debinding times are required (tens of hours) to prevent cracking, even for modestly thick parts.

Several attempts at direct deposition processes of ceramics with little or no binder have been attempted to reduce processing times. These methods rely on an intense, localized heat source such as a focused laser beam to produce sufficient heat to melt or densify the powder to near full density. This presents another extremely challenging problem because 1) sintering times must be on the order of seconds to make scanning of large 3-D parts practical; such fast sintering times may not be plausible for completely densifying many technically relevant ceramics via conventional sintering; and 2) for those ceramics where rapid sintering or melting is possible, the high temperatures required to densify a ceramic combined with the large Young's modulus, poor thermal conductivity, low fracture toughness, and extreme thermal gradients near the laser beam results in severe thermal shock of the ceramic. Thus, this approach has not been successful to date. Figure 3 contrasts the temperatures at which typical technical ceramics melt compared with polymers, metals, and glasses. External heating of the powder bed has been attempted to reduce thermal gradients associated with laser processing, but the very high preheating temperatures required and resulting microstructural coarsening preclude the use of this technique for most ceramic compositions.

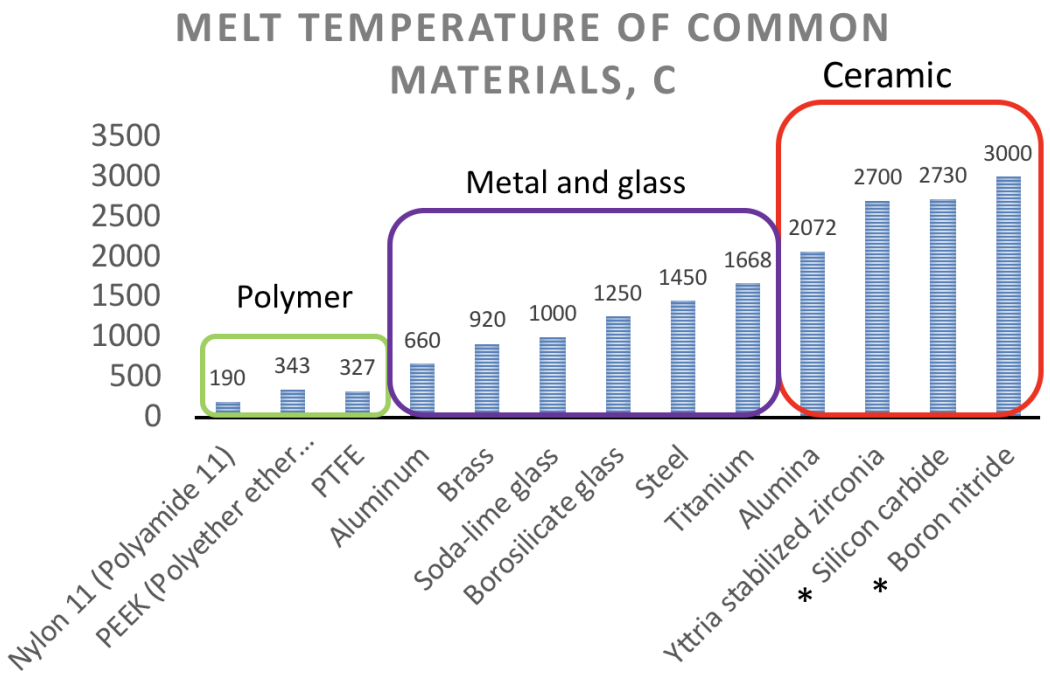

*Note: Silicon carbide and boron nitride do not melt.

Fig. 3 Melt or decomposition temperatures of typical polymers, metals, glasses, and ceramics

4. Flash Sintering Overview

Electric-field-assisted sintering has experienced a rapid increase in interest due to its ability to dramatically lower sintering temperatures and increase sintering rates compared with conventional sintering. Two types of electric-field-assisted sintering experiments have been demonstrated: 1) spark plasma sintering, where sintering occurs within a die at high pressure, and 2) flash sintering, where the field is applied to an otherwise bare specimen using electrodes. The simpler, two-electrode flash sintering process is the focus of this work. Although the precise mechanisms that cause the electric field to increase sintering kinetics during flash sintering remains controversial, it has been demonstrated that sintering temperatures can be hundreds of degrees lower than for conventional sintering, and sintering times can be reduced from hours to seconds.

Figure 4 shows the furnace-based flash sintering equipment. A dogbone-shaped sample is suspended in a tube furnace with platinum wires connected to the positive and negative terminals of a DC or AC power supply. The furnace is heated to the point at which current begins to flow through the sample. At that point, the ceramic part densifies completely, as in Fig. 5.

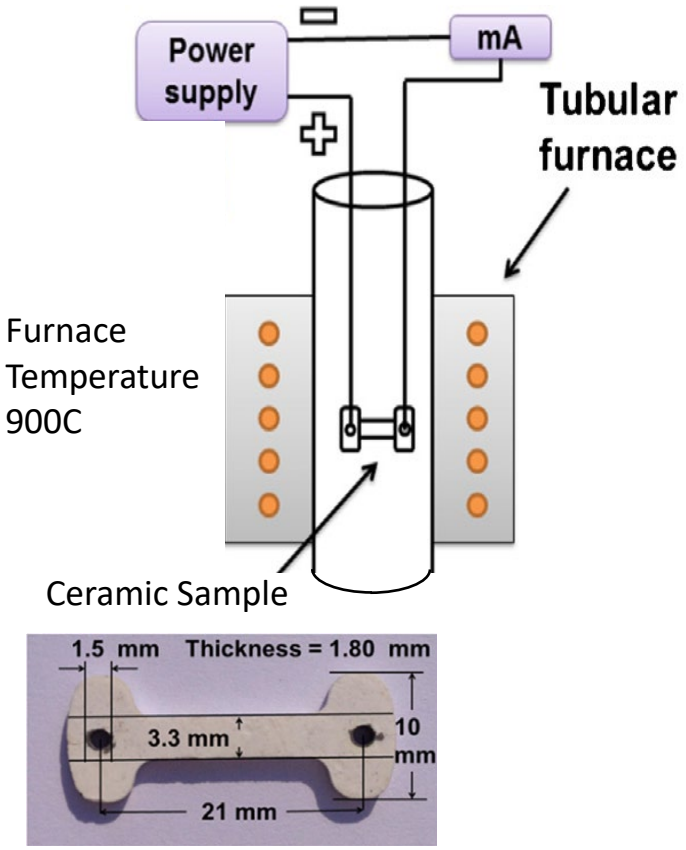

Fig. 4 Furnace-based flash sintering apparatus and sample

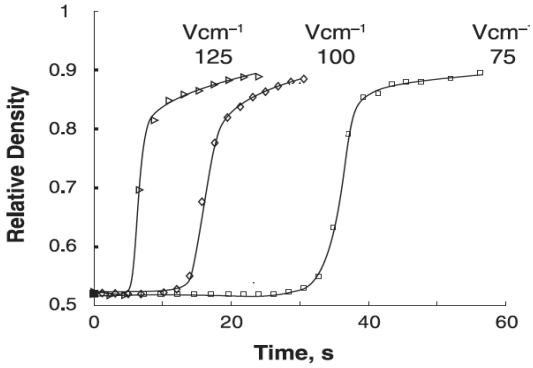

Fig. 5 Densification vs. sintering time for flash sintering at three different DC-applied electric fields[1]

5. Additive Manufacturing of Ceramics by Laser Flash Sintering

Here we propose an alternative two-part approach (summarized in Fig. 6) to additive manufacturing of ceramic parts in which a laser is first used in conjunction with an electric field to induce initial stage sintering of the part to a sufficient degree that necks are produced between the particles and the part will

hold together wherever the laser was scanned over the powder bed. The sample is then overcoated with fresh powder and the laser is scanned over the surface again. This process is repeated until a bulk part is fabricated using this layer-by-layer approach. In the second step, the partially sintered part is removed from the powder bed, the loose powder is gently removed to expose the partially sintered part, and a postprocess conventional sintering treatment in a furnace or a conventional flash sintering treatment is performed to complete densification.

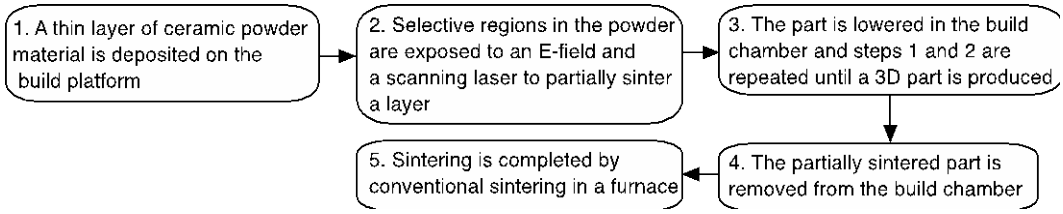

Fig. 6 Flow chart showing steps in proposed laser flash sintering process

The advantages of this method of additively manufacturing ceramics are 1) little or no binder is left following initial stage sintering, thus relatively thick parts can be produced without complications from pyrolysis; 2) scan speeds can be high, enabling rapid part manufacture since only partial sintering is required; 3) the laser power and associated temperature gradients are reduced compared with those needed for complete densification; 4) because the amount of shrinkage experienced during initial stage sintering is dramatically reduced compared with that required for complete densification, the strains experienced during scanning are dramatically reduced; 5) because the ceramic is only partially sintered, it is much more resistant to thermal shock; and 6) unlike indirect methods, complicated support structures are not required. Taken together, these advantages will allow much larger parts to be produced far more quickly than current indirect AM processes.

Table 1 lists the components of the ceramic slurry used in the sintering process.

Table 1 Ceramic slurry composition

Component	Function	Weight %	Volume %
8% yttria-stabilized zirconia (YSZ; Tosoh TZ8Y)	Ceramic	69.4	24.6
Ethyl alcohol	Solvent	23.9	63.2
Lubrizol Solsperse 41000	Dispersant	2.9	5.6
Kuraray Mowithal B30H (polyvinyl butyral)	Binder	1.7	3.3
Polyethelene glycol (300)	Plasticizer	1.7	3.3
Santicizer 160 (butyl benzyl pthalate)	Plasticizer	0.4	0.8

Note: The ethyl alcohol evaporates fully after the slurry is dispensed.

Organics in the slurry must be removed by heating above the decomposition temperature of the polymers. The decomposition temperature range of the polymer mixture in the slurry was measured by thermogravimetric analysis (TGA). A small sample of material is slowly heated (10 °C/min) and continuously weighed during the temperature ramp. The polymers will decompose into gases in the air atmosphere, reacting with oxygen to form gases such as carbon dioxide and carbon monoxide. When the mass no longer changes with additional heat, the pyrolysis is complete.

Figure 7 shows the TGA curve for the slurry used in these experiments. The slurry was dried in air overnight, during which the ethanol solvent evaporated. The remaining slurry then consists of the binder, plasticizers, dispersant, and the yttria-stabilized-zirconia (YSZ) powder. The polymers are engineered to oxidize easily and completely in an air atmosphere. They break down at relatively low temperatures and completely volatilize into gases. After an initial small slope, the sample begins a steady loss of mass due to decomposition of the polymers into gaseous products starting at 180 °C. The loss of mass is completed by 425 °C. The remaining mass above 425 °C consists of YSZ powder. Note that the YSZ is inert at these temperature ranges. After the ethanol is evaporated, the data show that the composition of the slurry by percent mass is 90% YSZ ceramic and 10% polymer. A blank consisting of an empty crucible was run to account for any outgassing and loss of adsorbed moisture from the crucibles. This blank was subtracted from the raw data. A student repeatedly bumped the table, causing the irregular peaks in the data. These irregular peaks were not present in the raw data of the sample.

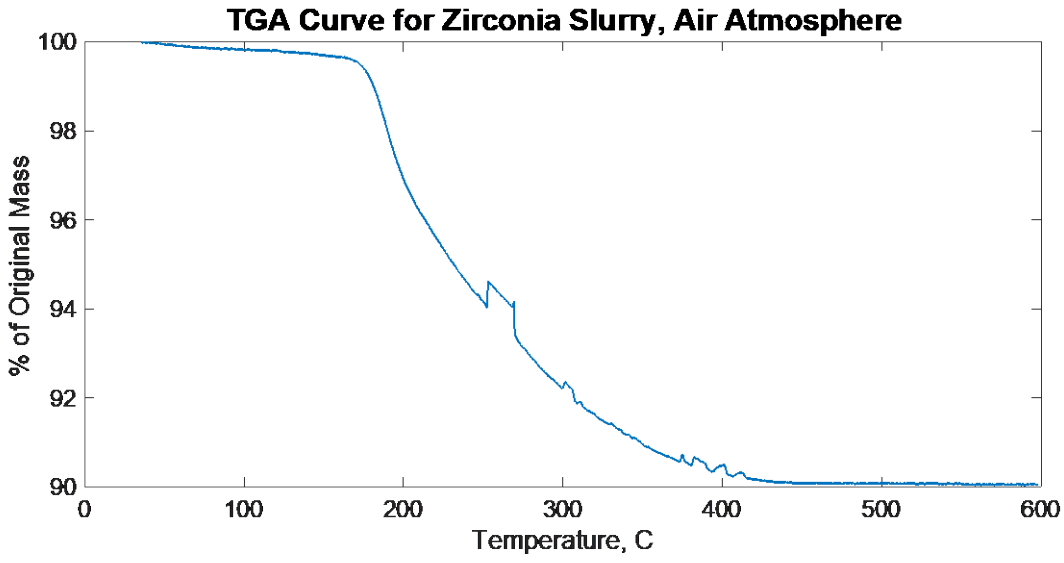

Fig. 7 TGA of zirconia slurry

6. n-Scrypt Equipment Overview

Figure 8 shows the n-Scrypt tool array, YAG, laser, and other components of the experimental setup.

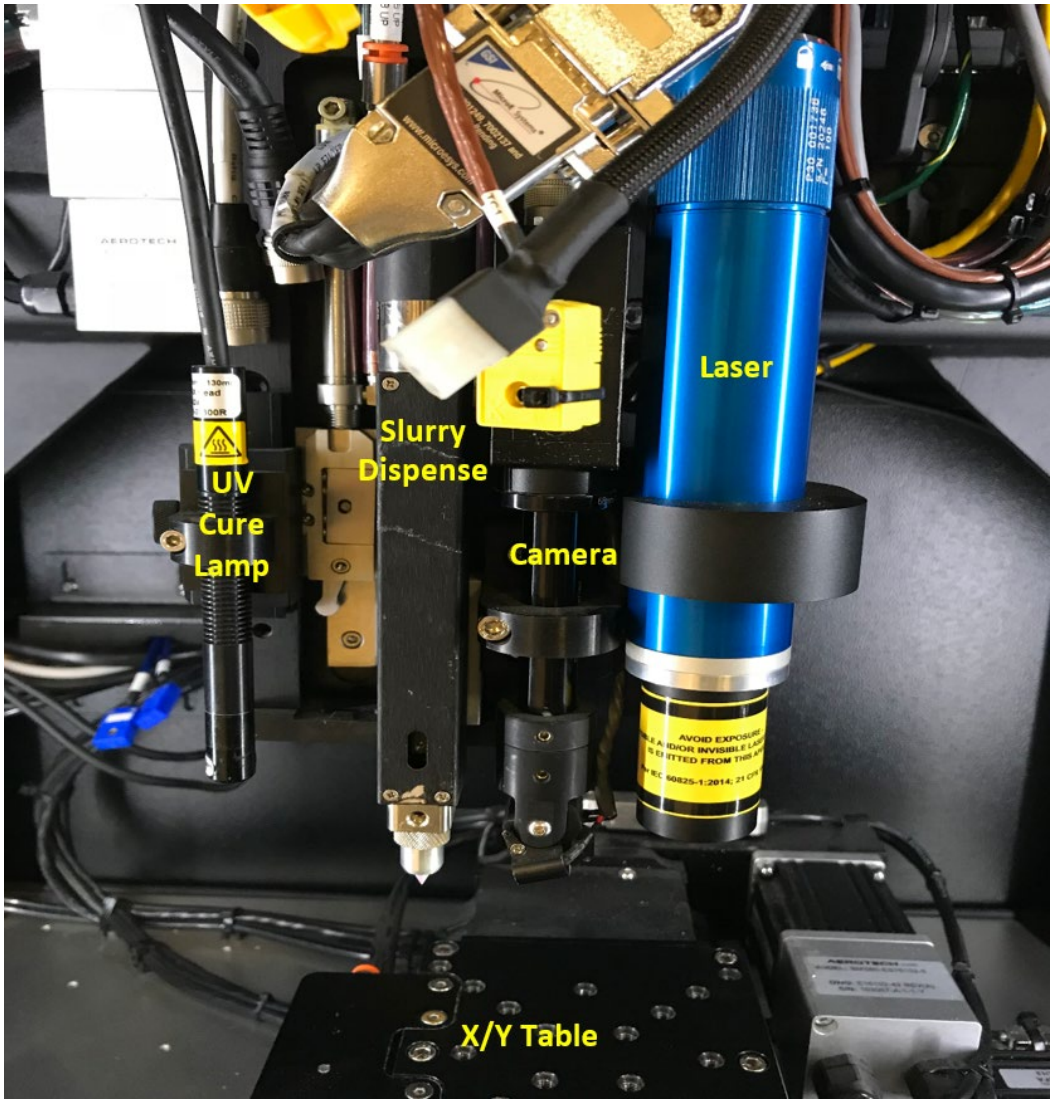

Fig. 8 n-Scrypt machine tool array and x/y table with YAG laser, process monitor camera, slurry dispense tool, and UV cure lamp. Fused deposition modeling head is not installed. The tool array is stationary in the x/y direction and moves only in the z (vertical) direction.

6.1 Sample Build Surface

The sample build surface is fastened to the x/y table of the n-Scrypt with bolts. Two sample build surfaces were used. Both used individual disc-like steel stubs that screwed into a flat plate. They were designed to be removable so that they

could fit directly into the Jeol scanning electron microscope (SEM) on campus for analysis. The larger of the two plates was designed to fasten on top of the x/y table heater bed that is an option in the n-Scrypt. The heater bed can be used to accelerate the drying rate of the solvent (ethanol) in the ceramic slurry between dispensing and lasing. Both the heated and nonheated fixtures are attached to a precision x/y table that has high accuracy in both speed and precision of travel.

A photograph of the heater bed sample array is shown in Fig. 9. Drawings for the sample plates are shown in Figs. 10 and 11.

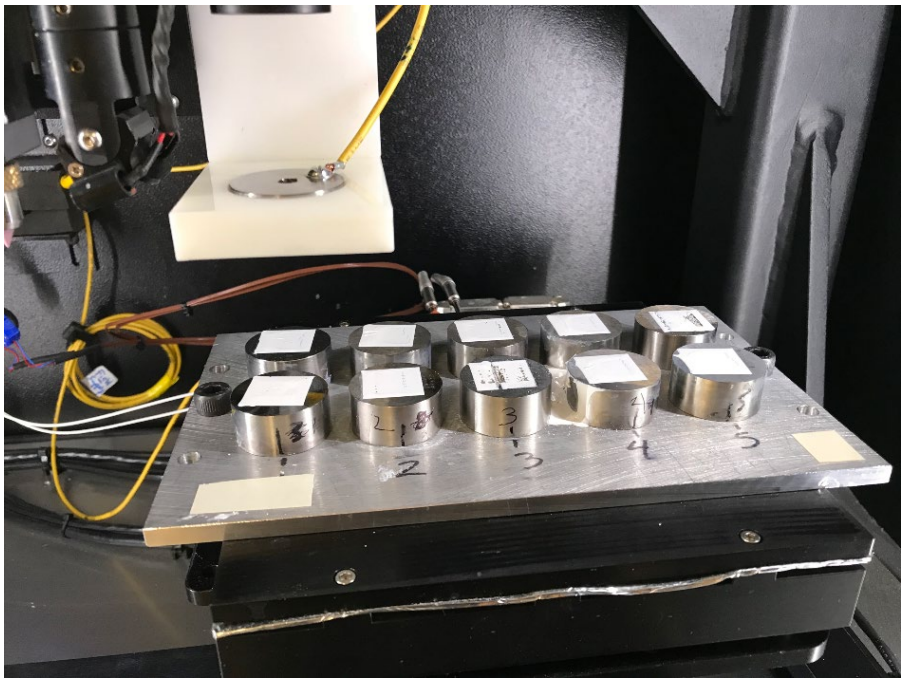

Fig. 9 Sample build plate fastened to the x/y table with part bed heater installed. Ten different samples are located on the build surface. A large square has been dispensed onto each sample surface.

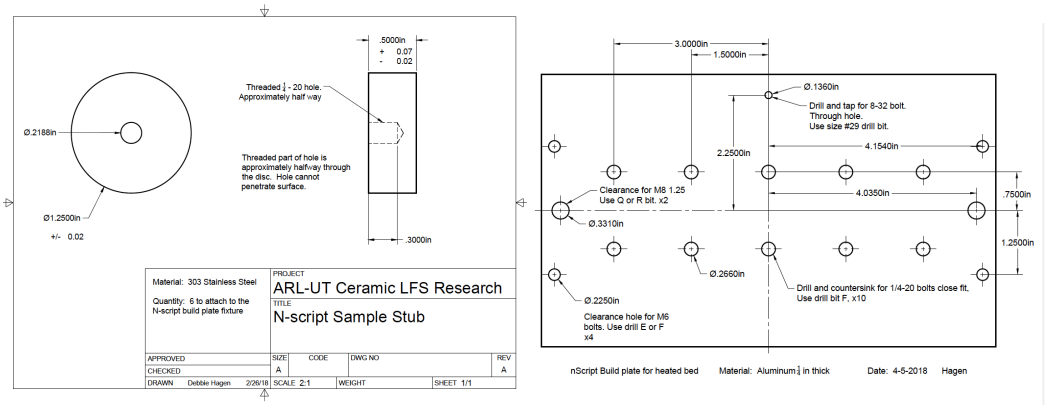

Fig. 10 Drawings for the sample stubs (left) and the sample build plate for the heated bed (right). Stubs fasten to the build plate from below with bolts.

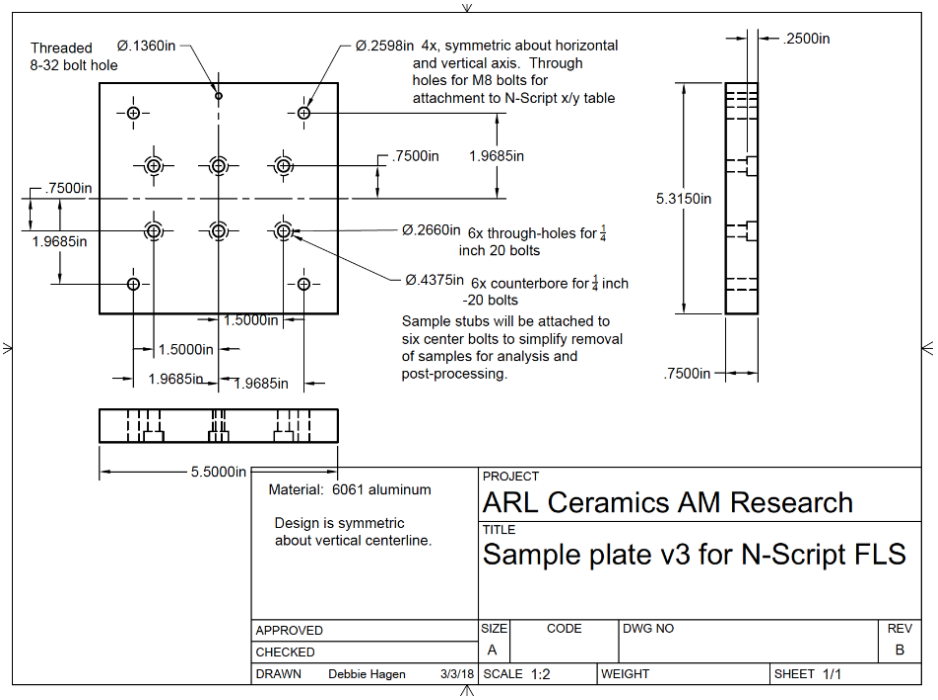

Fig. 11 Sample plate for n-Scrypt, non-heated bed

6.2 Dispense

The n-Scrypt is equipped with a "Smart-Pump" pneumatic dispensing tool designed to dispense inks and slurries in single or multiple layers. Multilayer parts are shown in Fig. 12. The mechanism is shown in Fig. 13. A stepper motor drives a lead screw that drives an attached valve rod (not shown) up and down in the vertical direction. The valve rod has an O ring that seats against the opening of the pen tip to control the flow of ink or slurry out of the ceramic pen tip, shown in Fig. 13.

Fig. 12 Dispensed multilayer parts assembled with the ARL n-Scrypt

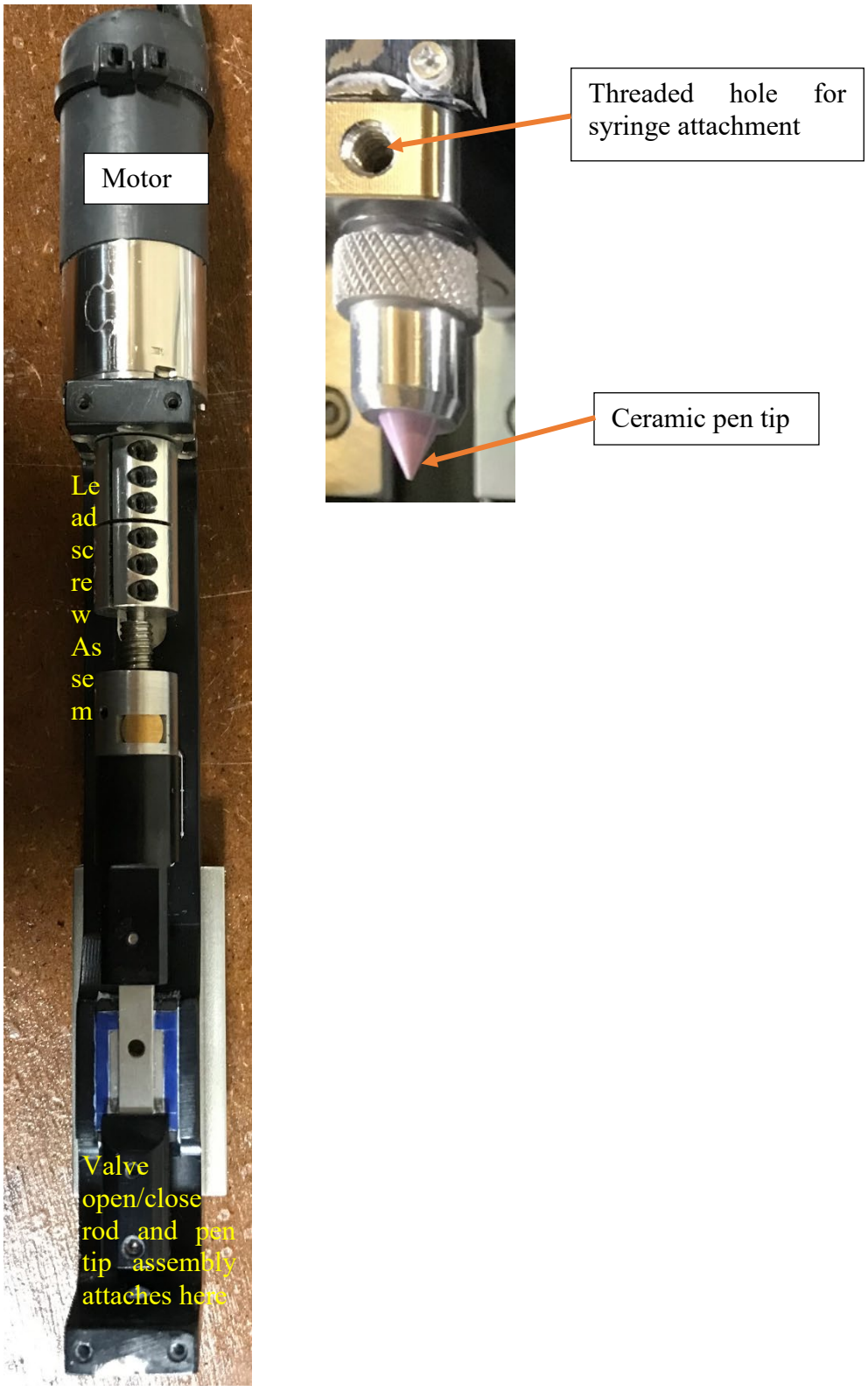

Fig. 13 Pen tip assembly for n-Scrypt dispensing[1]

A syringe screws into the threaded hole in the pen tip assembly, shown in Fig. 13. Air pressure is applied to the back of the syringe. The air pressure is designed to push a free-floating plastic plunger inside the syringe. As the plunger moves, it pushes slurry or ink into the pen tip.

The rate of slurry dispense will depend on several controllable variables, which include the following:

- Diameter of the pen tip opening
- Air pressure applied to the syringe plunger
- Rheology (e.g., viscosity) of the ink or slurry
- Amount and speed of the travel of the valve rod
- Speed of the x/y table (and therefore the rate of travel of the sample) under the pen tip
- Gap between the pen tip and the sample
- Wait times between opening of the valve rod and initiation of motion of the x/y table.
- Surface tension of fluid, which depends on both the slurry or ink and the material type and surface finish of the sample

In addition, the following uncontrolled process variables significantly affect the dispense quality and dispense rate:

- Sticking of the plunger within the syringe
- Drying of the slurry or ink in the pen tip, resulting in partial or total obstruction of the pen tip opening
- Changes in viscosity due to shear rate of the slurry or ink as it flows through the pen tip
- Air bubbles in the slurry or ink

The first three of these were major issues for print quality in the parts, causing uneven or blocked dispense, height and width variations across the dispense area, and unpredictable and highly irregular printing, as shown in Fig. 14. The variations can be minimized by increasing the air pressure to at least 70 psi, which helps with plunger sticking but does not eliminate it. Scrubbing the pen tip with a swab wetted with ethyl alcohol prior to dispensing helps to dissolve dried slurry or ink in the pen tip. The larger-diameter pen tip opening also helps to reduce the

amount of shear thinning behavior in the slurry because it reduces the shear rate of the material flowing through the nozzle. Ultimately, the process can be better controlled by replacing the pneumatic system with a positive displacement mechanical pump.

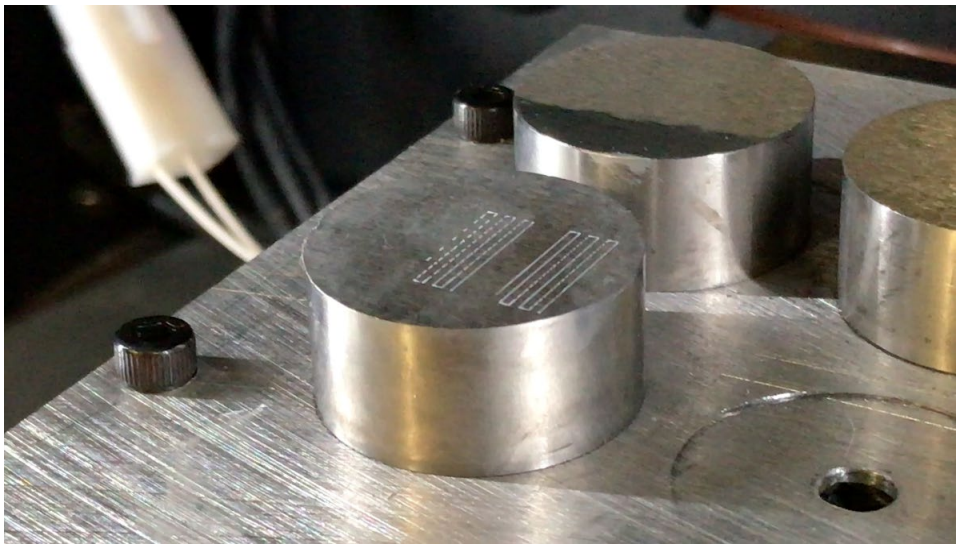

Fig. 14 Still photo from a video of dispense of a serpentine pattern of ceramic slurry with n-Scrypt. Two layers have been dispensed.

6.3 Laser

The YAG laser in the n-Scrypt has a wavelength of 1 µm. It is capable of generating 150 W of power and is controlled with software that synchronizes the motion of the x/y table with the laser on/off and power settings through use of a script (Fig. 15).

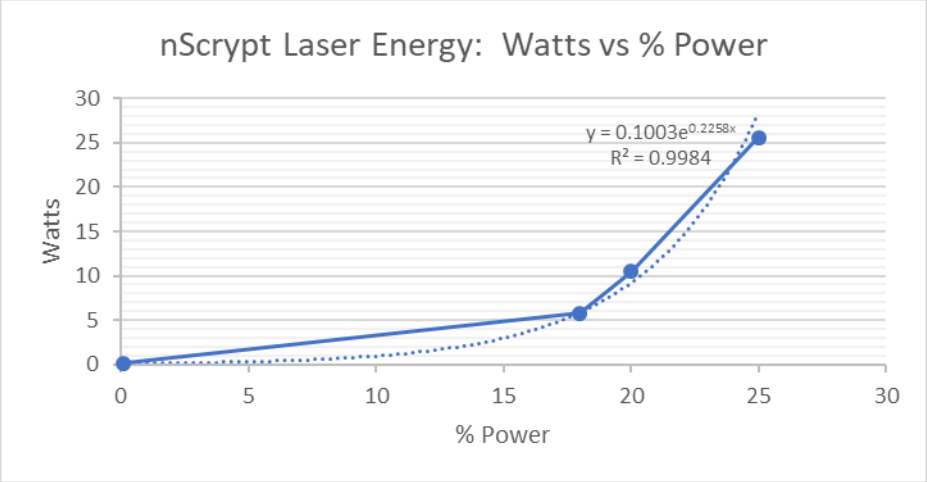

Fig. 15 Laser power vs. percent power curve fit

6.4 Application of DC Electric Field: Electrode and Electrode Holder

The flash laser sintering process uses the energy of an electric field in combination with laser energy to fuse the ceramic particles. A custom electrode and electrode holder was designed and fabricated for the part, shown in Fig. 16. There is literature evidence that there is a field effect with furnace sintering even when the electrodes do not directly touch the part. To maximize flexibility, the electrode was designed to be a noncontact electrode.

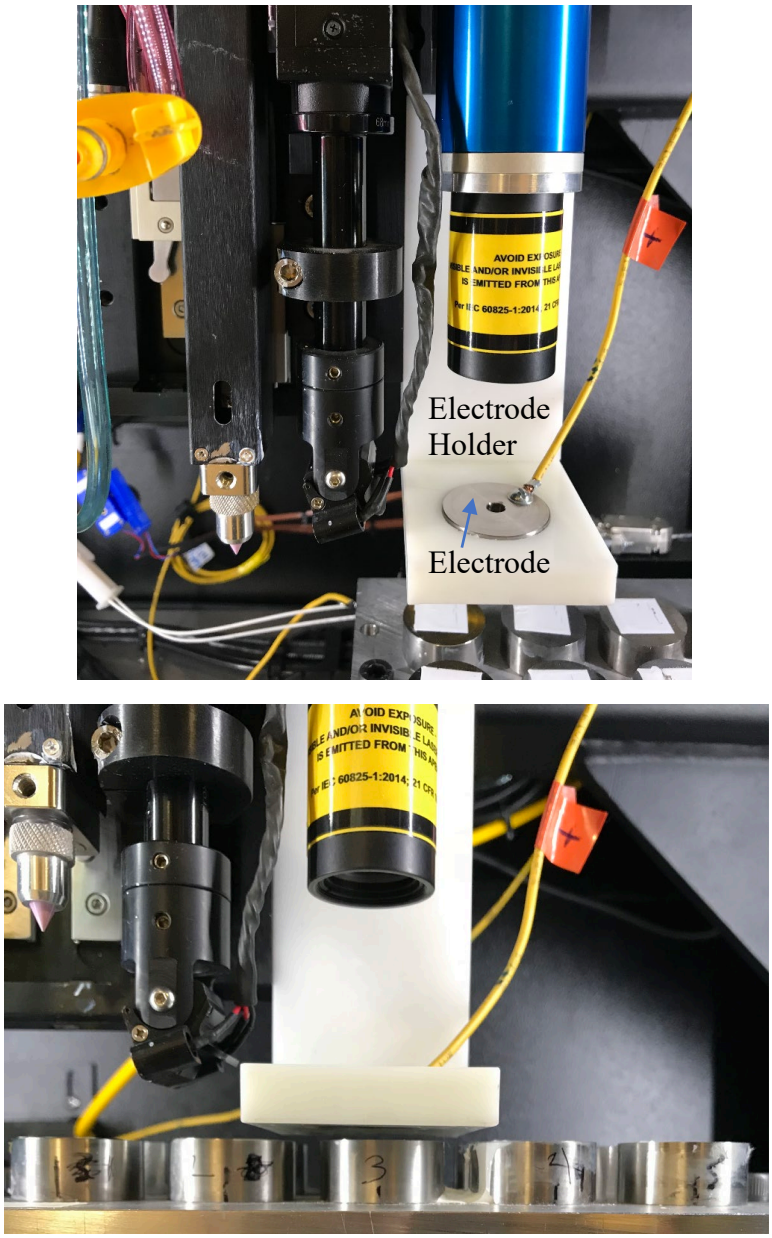

Fig. 16 Two views of electrode holder and electrode installed in the n-Scrypt

A DC power supply is connected to the positive and ground terminals of the system. The positive electrode is suspended between the laser and the workpiece. The laser beam travels through a hole in the electrode. The bottom of the electrode can be at various heights above the sample to vary the electric field. Figure 17 show the electrode to sample gap of 2.5 mm that was used for this evaluation. The electrode is constructed of stainless steel, and the electrode holder is a two-piece assembly constructed of insulating polymer material fastened with nylon bolts. The metal workpiece is connected to ground potential, and the electrode is connected to the positive terminal of the external DC power supply.

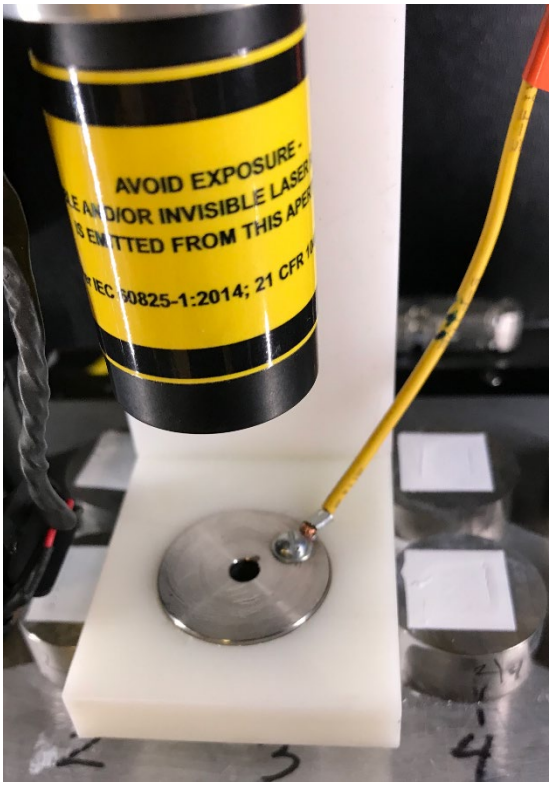

Fig. 17 Electrode holder in the typical configuration for lasing. Note the small gap between the bottom of the electrode holder and the top of the build area.

Figure 18 shows design drawings for the electrode, and Fig. 19 shows drawings for the electrode holder parts and assembly. The electrode placement within the electrode holder was determined by lasing a small marker hole in the top of the plastic to use as the center point of the drill holes that the steel electrode fits within. This maximized the placement accuracy for the electrode with respect to the laser beam.

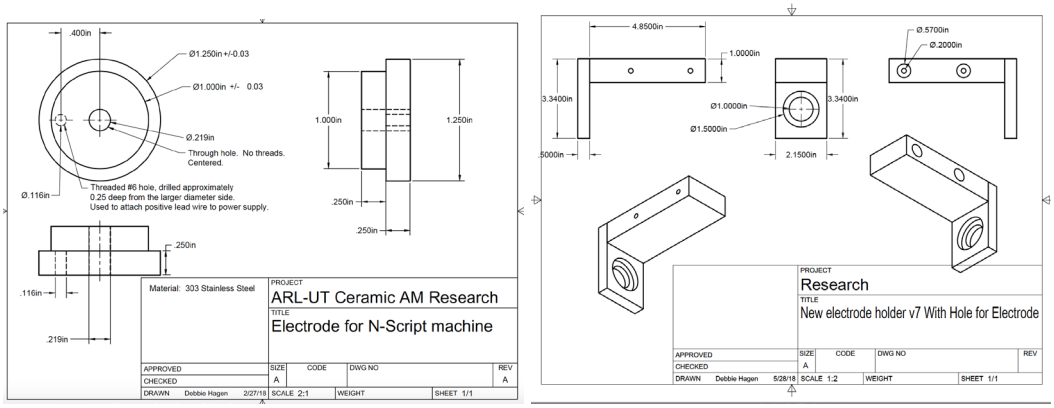

Fig. 18 Drawings of electrode for n-Scrypt and the electrode holder assembly

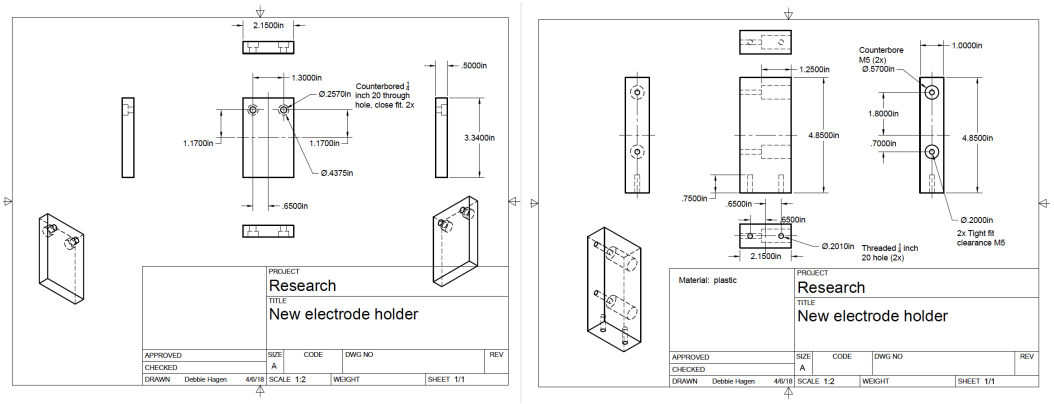

Fig. 19 Drawings for the two parts that make up the electrode holder assembly. These two parts are fabricated from nonconducting polymer material and fastened with nonconducting nylon bolts.

6.5 Atmosphere and Ventilation

The n-Scrypt is equipped for an air atmosphere that is vented outside of the building. The n-Scrypt is not equipped for inert atmospheres or vacuum.

The National Fire Protection Association 86 Standard for Ovens and Furnaces, Appendix D,[2] method was used to calculate the solvent safe minimum ventilation rate for flammable solvent vapor dilution. Based on a maximum of a cubic centimeter per minute slurry deposition, the minimum airflow rate for safe dilution of a worst-case solvent of 50% methyl ethyl ketone and 50% ethyl alcohol was 0.042 cm^2/min. The actual ventilation rate for the n-Scrypt is 8 cm^2/min, substantially over the required minimum.

6.6 Heaters

A heater plate is available for the n-Scrypt that can heat the sample bed for faster evaporation of solvents from slurries or inks. The heater bed was not used in this feasibility evaluation but its use could decrease the build time by accelerating drying of any solvents from inks or slurries dispensed in the n-Scrypt.

7. Ceramic Materials

Oxide materials were the preferred ceramics for this feasibility study because they are easily processed in an air atmosphere without degradation. Two technical oxide ceramics were investigated for this study: aluminum oxide (alumina) and YSZ. Note that zirconia undergoes a destructive phase change when cooled from sintering temperature to room temperature, and zirconia is therefore commonly doped with a cation that replaces a certain percentage of zirconium ions for the purpose of stabilizing one of the natural phases of zirconia. In this evaluation, the fully stabilized cubic form was used, which has 8% yttria incorporated into the zirconia.

Both ceramics are widely used and have unique properties useful to a variety of applications. The typical properties of both of these ceramics are listed in Table 2. For our particular application, the absorption, reflection, and transmission properties of 1-µm wavelength energy is an important property as well. Figure 20 shows the absorptivity, alpha, of 0.5- to 3-µm wavelength energy for alumina. The absorptivity is very low. The absorption increases with temperature, but even at 1700 °C it absorbs less than 4% of energy per centimeter of thickness.

Table 2 Properties of alumina[a] and 8% YSZ[b]

Property	Units	99.9% Alumina	8% YSZ
Flexural strength, MOR (20 °C)	MPa	350–600	180–193
Fracture toughness, K_{IC}	MPa m1/2	4.0–5.0	4,0
Thermal conductivity (20 °C)	W/m K	28–35	2.5
Coefficient of thermal expansion	1 × 10–6/°C	8.0–8.5	10.5–11.0
Maximum use temperature	°C	1750–1800	1800–2400
Dielectric strength (6.35 mm)	ac-kV/mm	8.7	…
Dielectric loss (tan δ)	1 MHz, 25 °C	10-4 to 10-3	…
Volume resistivity (25 °C)	Ω-cm	1014 to >1015	108–1014

[a]https://www.coorstek.com/english/materials/technical-ceramics/alumina/alumina-999-100/
[b]https://www.coorstek.com/english/materials/technical-ceramics/zirconia/fully-stabilized-zirconia/
Note: MOR = modulus of rupture

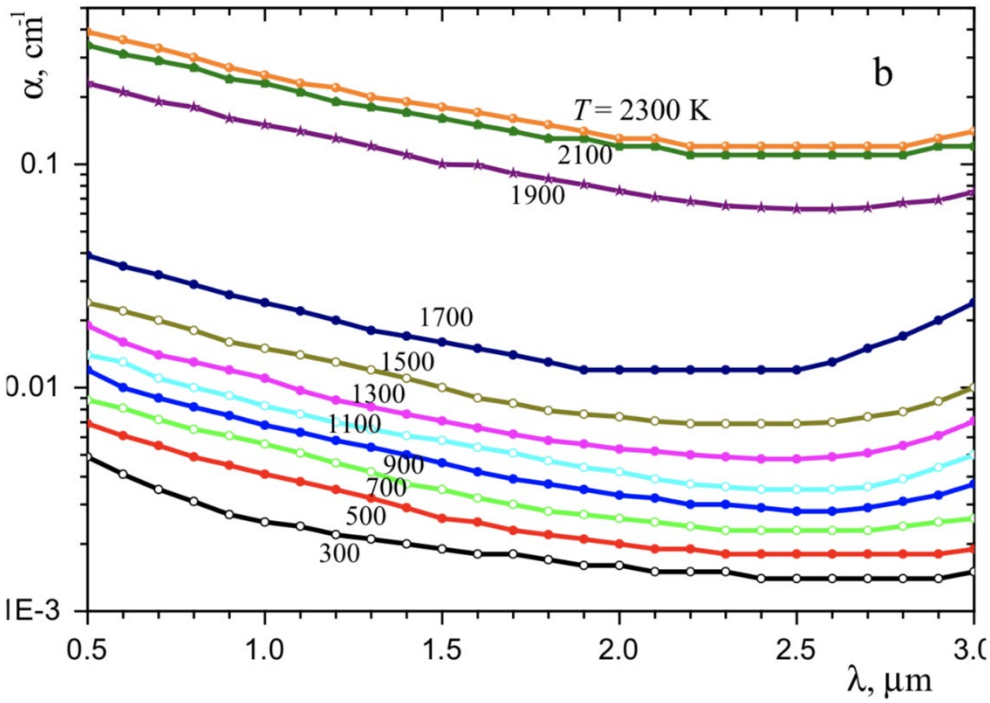

Fig. 20 Absorptivity of energy for alumina ceramic at various temperatures and wavelengths. Absorptivity is on the y axis and wavelength is on the x axis.

We attempted to increase the absorptivity of the alumina to the 1-μm wavelength by doping with iron, which causes alumina to turn a dark brown color in large concentrations. The color change indicates that the doped alumina is absorbing in the visible portion of the energy spectrum and could possibly enhance the near-IR absorptivity. However, the doping process was not successful.

A search of literature data for all of the common ceramic oxides showed that as a material class they have very low absorption in the 1-μm wavelength region. The best option would be to process non-oxides, some of which absorb the 1-μm wavelength well. These ceramics, however, should be processed in an inert atmosphere, and the n-Scrypt is not currently equipped with that capability.

Nanoparticles scatter energy at a higher rate, so there is a higher chance of particles encountering multiple "hits" of laser energy due to high scattering. Zirconia is easier to sinter and easier to flash sinter with an electric field, so the feasibility was done with zirconia 40-nm-diameter powder, which will be highly scattering compared with solid zirconia. Figure 21 shows the absorptance, normal-hemispherical reflectance, and transmittance of a porous 8% YSZ sample of zirconia. Note that the absorptivity is below 4% at the lower-wavelength (2-μm) end of the graph, and that reflectance, which is related to scattering, is high.

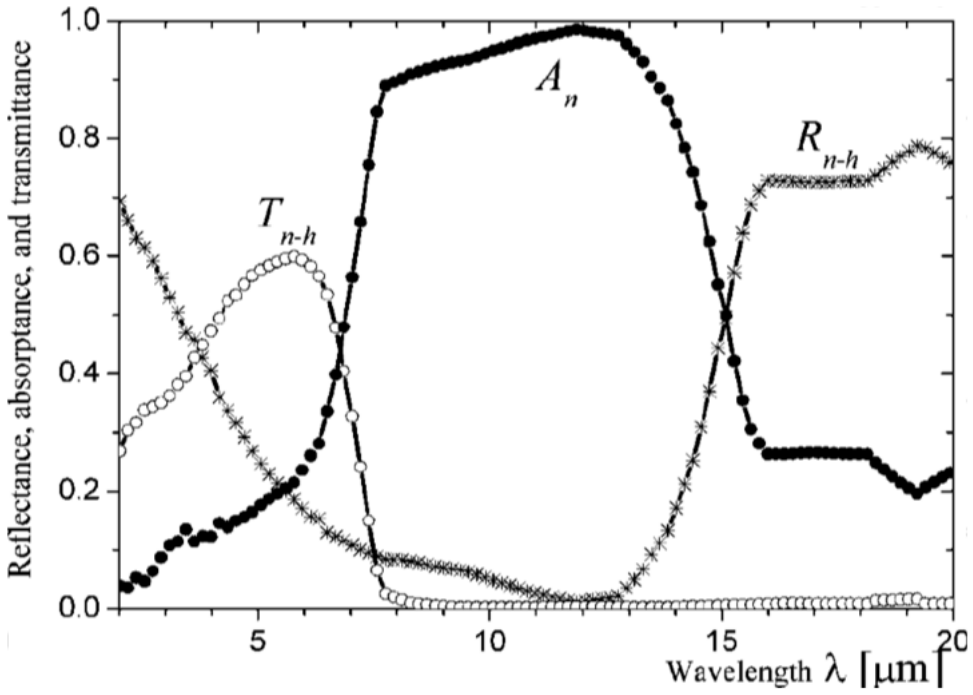

Fig. 21 Normal hemispherical reflectance (R), transmittance (T), and normal absorptance (A) for porous 8% YSZ ceramic sample at room temperature

Additional data, shown in Fig. 22, include temperature dependence. The data are graphed in terms of absorption coefficient and scattering coefficient from a minimum of 1-μm wavelength to a maximum of 8 μm. These data are from zirconia thin films of the same composition of 8% YSZ, and show the same trend of high scattering at 1 μm and low scattering at 8 μm combined with low absorption at 1 μm and high absorption at 8 μm. Just as with alumina, the absorption increases with increasing temperature.

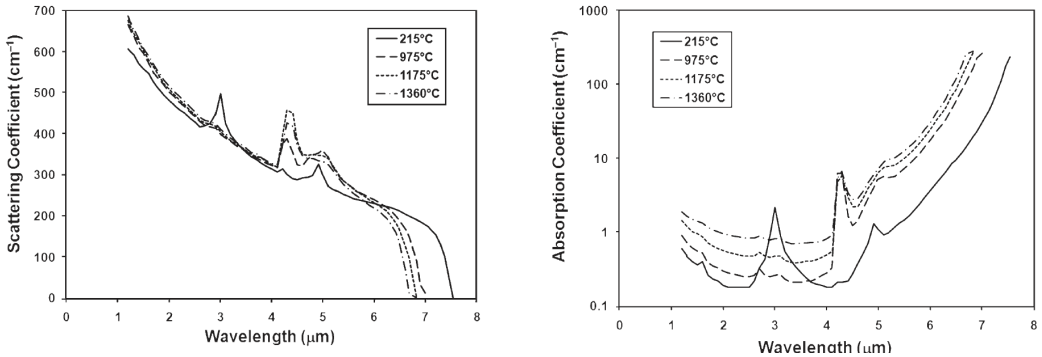

Fig. 22 Scattering coefficient and absorption coefficient for 8% YSZ thin films measured at various temperatures and wavelengths

8. Experimental Data and Results

8.1 Nonrastered "Dot" Laser Test on Single-Layer Slurry

The first experiment was to test whether the laser had any effect on the slurry, knowing that the absorption of 1-μm wavelength laser energy was low for oxide ceramics. A single point was hit with the laser for approximately 2 s at various powers. The effect was observed by visual inspection and SEM. Nonmagnified parts after lasing are shown in Fig. 23.

Fig. 23 Visual appearance of laser "dot" experiment. The two samples at the lower right were not lased.

No obvious visual changes can be seen at low powers. Black dots can be seen at the higher laser powers, and the laser drills down into the stainless steel build surface at even higher laser powers.

The SEM photo in Fig. 24 shows that the high-power laser scans melted or vaporized the polymer, which appears white in the SEM images, resolidified as a spider-web-like fashion on top of the dispensed slurry. Higher powers create crater structures. The center of the crater, where the beam resided, generally had little to no zirconia powder or particles left, and frequently the ceramic was removed, leaving only the stainless steel of the build surface in the area of the beam center. Some debris can be seen at the bottom of the craters (Fig. 25). A glassy area is present in some of the craters, indicating temperatures

became very high (Fig. 26). Grain growth and recrystallization also occur at high powers in the crater areas. This shows that there is material removal and modification at high laser powers in spite of the low absorption of the ceramic. It might be possible to control the energy transfer from laser to ceramic in spite of the low absorption of 1-µm energy by oxide ceramics.

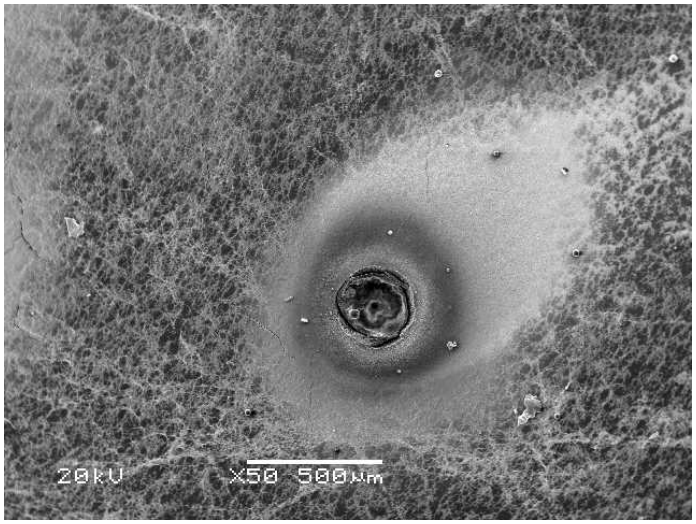

Fig. 24 White polymer web extends from crater created by the laser

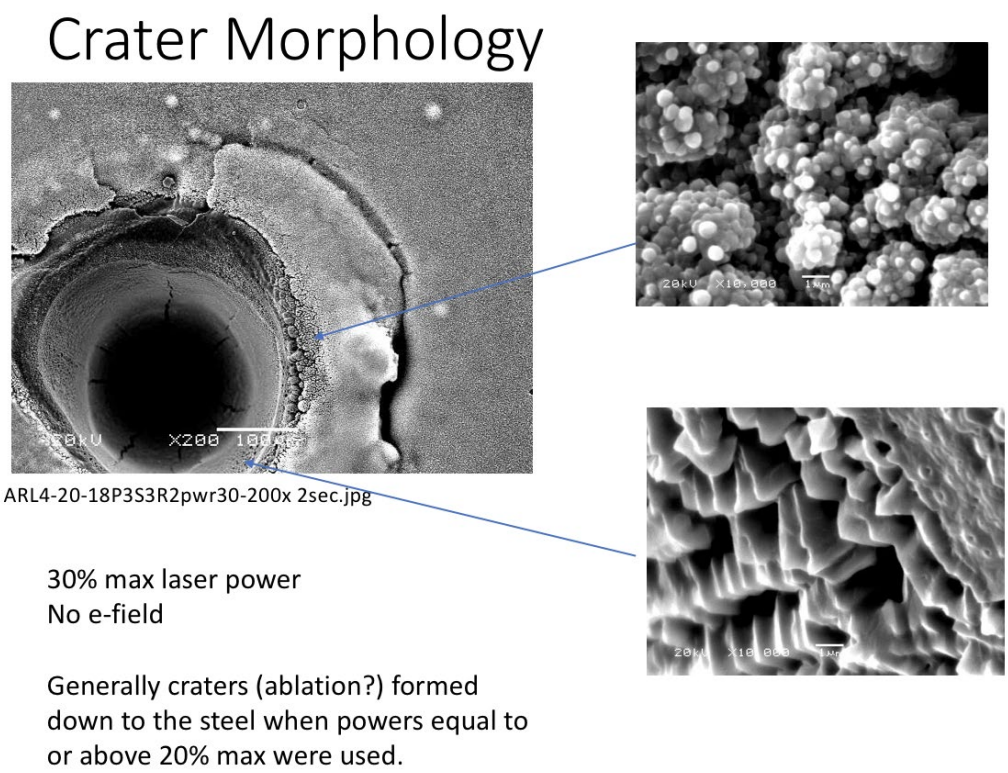

Fig. 25 Crater in zirconia slurry bed without glassy phase

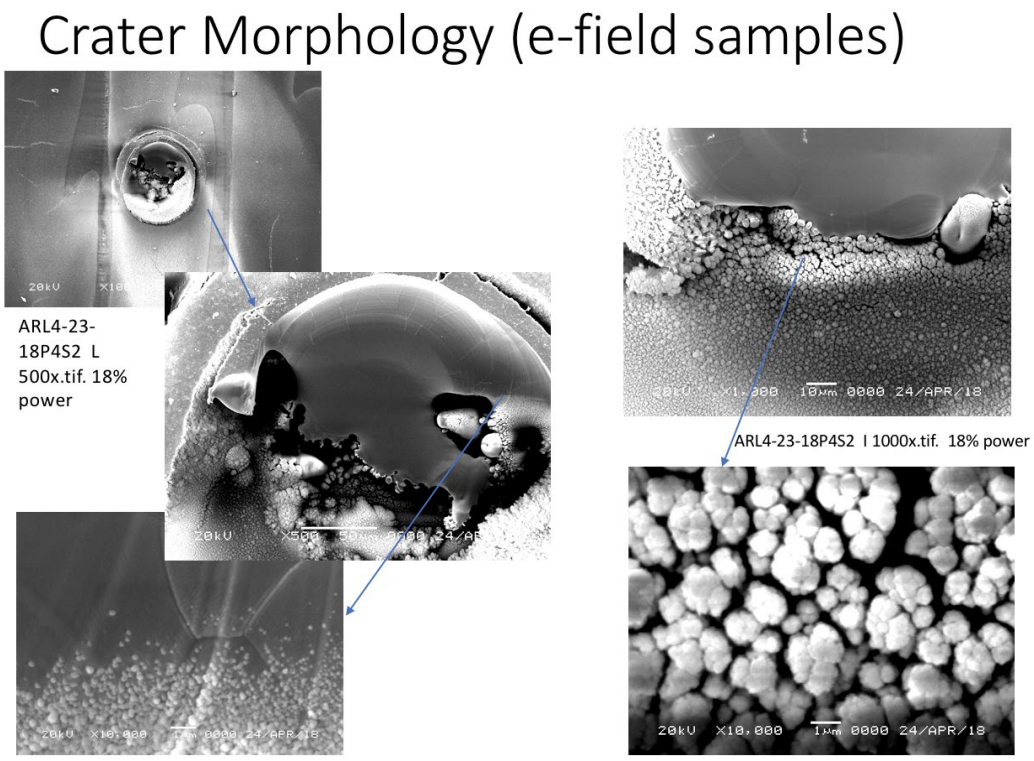

Fig. 26 Crater in zirconia slurry bed with recrystallized glassy phase

8.2 Single-Layer Parts: Laser Scanning Condition Test

Single-layer parts on a stainless steel base were built, testing different lasing conditions. The parts were examined with the SEM to identify parts that appeared to be sintering, but the technique was not quantifiable. It appears as if the first condition in Fig. 27 is more consolidated than the second condition, but the data are not quantifiable and inconclusive. The first condition is approximately three times the effective power density of the second condition. The SEM of the surface of the part is not sensitive enough to determine is necks are forming.

Surface appearance:
Without field With field

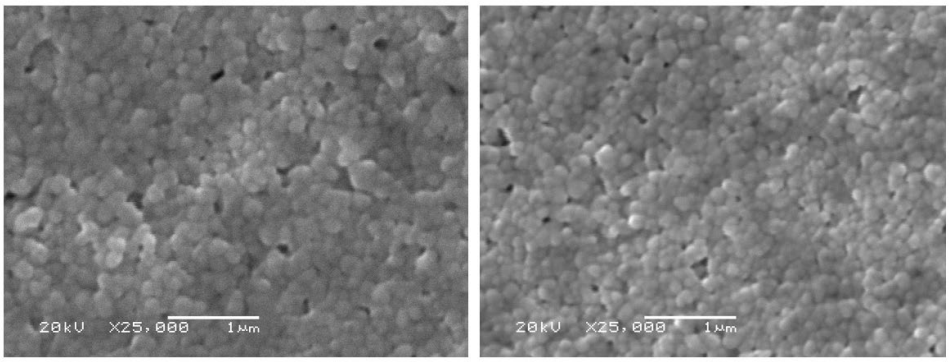

5-7-18-P9-S1R-25000x.tif

Laser power 20% (10.5 Watts)
Raster speed 100 mm/sec
YSZ slurry

5-7-18-P10-S1R-25000x.tif

300V/2.8mm gap => Field of 1000V/cm
Hatch Spacing 100 microns
(0.1 W/mm)

Surface appearance:
Without field With field

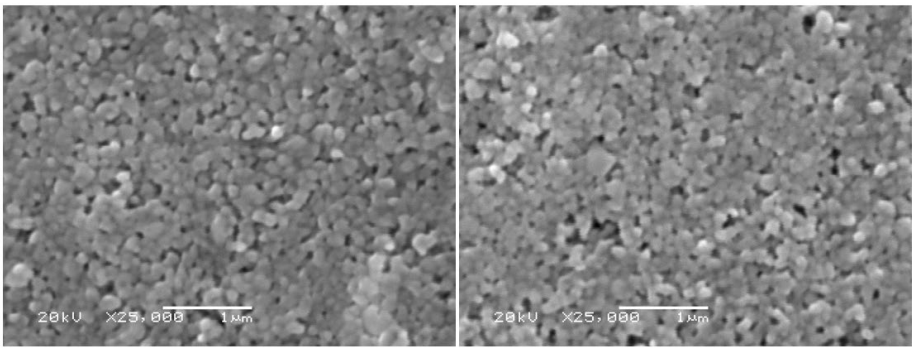

5-7-18-P9-S3R-25000x.tif

Laser power 12% (1.55W)
Raster speed 50 mm/sec
YSZ slurry. (0.03 W/mm)

5-7-18-P10-S3R-25000x.tif

300V/2.8mm gap => Field of 1000V/cm
Hatch Spacing 100 microns

Fig. 27 Surface scans of single-layer parts, top-down view, in high-magnification SEM. Top two photos are three times the energy density of the bottom two photos.

8.3 MultiLayer Parts: Cross Sections before and after Firing

Three-layer ceramic rectangles were built on the n-Scrypt with various laser scanning conditions based on the single-layer experiments. They were fractured in half and imaged with SEM prior to firing to determine layer to layer adhesion before firing. The other half of the samples were fired at the recommended firing conditions in a box furnace with air atmosphere. Ramp-up was 5 °C/min, firing temperature was 1450 °C with a soak time of 1 h, and ramp-down to room temperature was 10 °C/min.

All lasing conditions with and without an electric field produced similar results for cross-section fracture surfaces before furnace firing. Typical SEM images are shown in Fig. 28. Delamination can be seen between layers at low magnification, and higher magnification shows that large quantities of polymer (binders and plasticizers) remain in the dispensed and lased slurry. Both the delamination and the large amount of polymer indicate that the laser was not providing enough energy to sinter the full layer. The layer thickness increases with each layer due to the need to place the slurry-dispensing pen tip at the highest point of the previous layer.

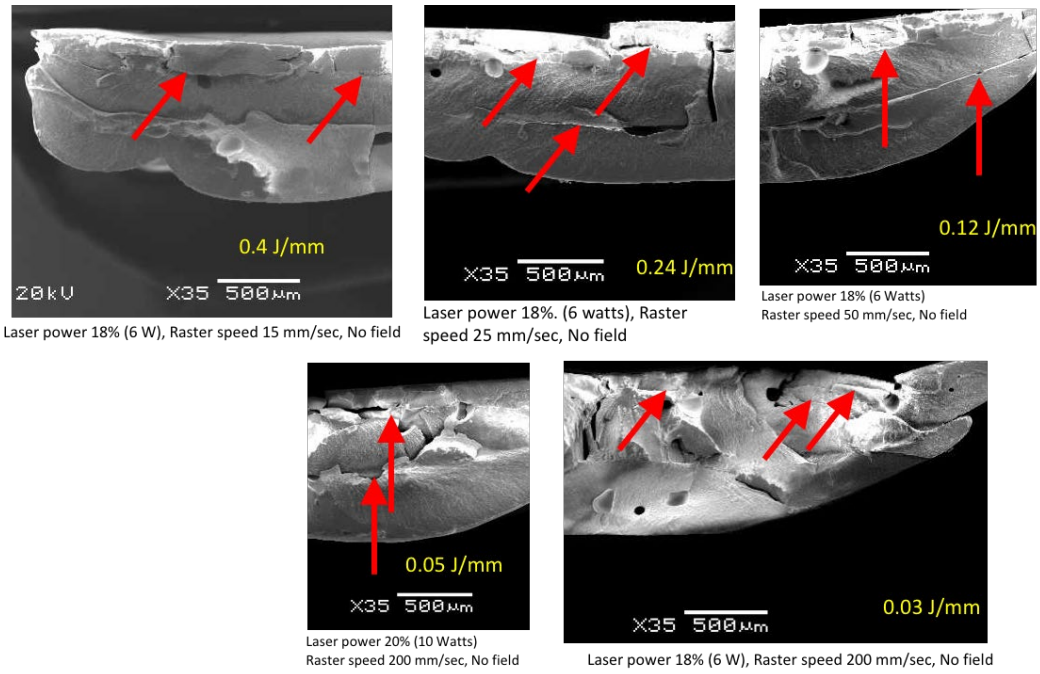

Fig. 28 Unfired cross sections of fracture surface. The "top" of the part is facing down in all of these images. Red arrows point to separation between dispensed layers.

The other half of the fractured samples were furnace-fired to the recommended time and temperature for zirconia. These parts were cross-sectioned and polished. SEM shows that the layers are fused together after furnace firing, and the samples generally have very few voids or no visible voids. Polished cross sections after firing are shown in Figs. 29 and 30. There is not a significant difference in the cross-section appearance of the ceramic parts based on the lasing conditions, which were low energy based on damage to the parts at high energy or the application of electric field.

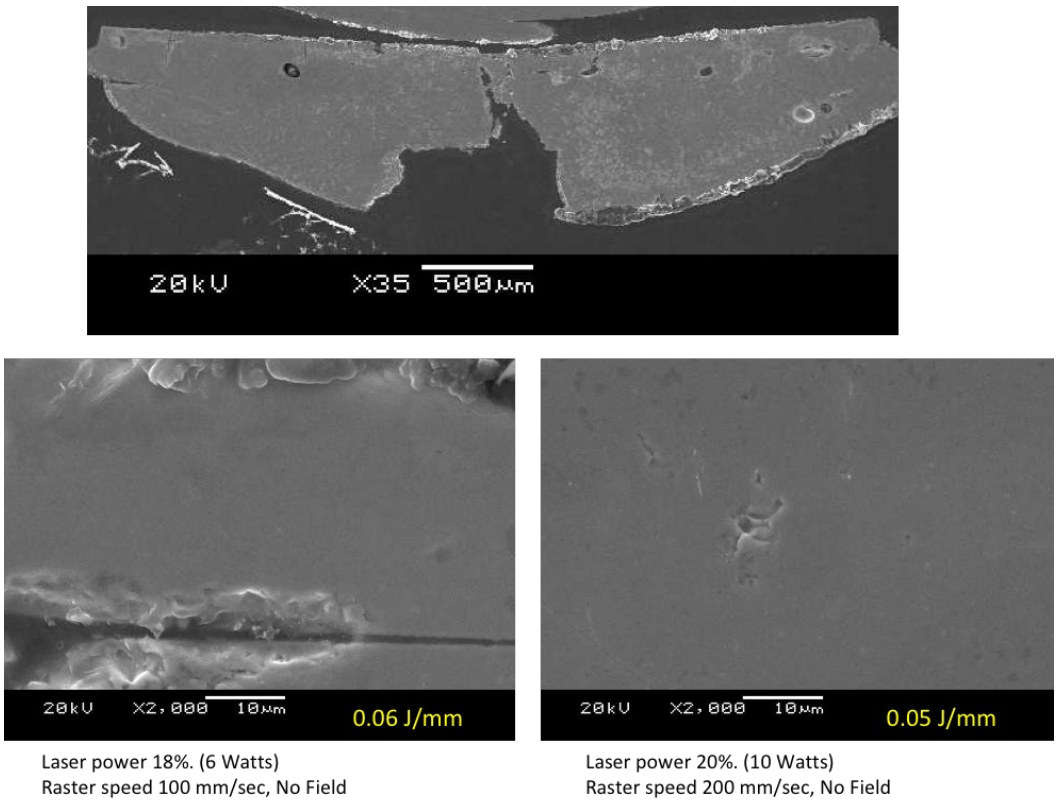

Fig. 29 Polished cross section of three-layer part after furnace firing. Left and right side of the part have different lasing conditions.

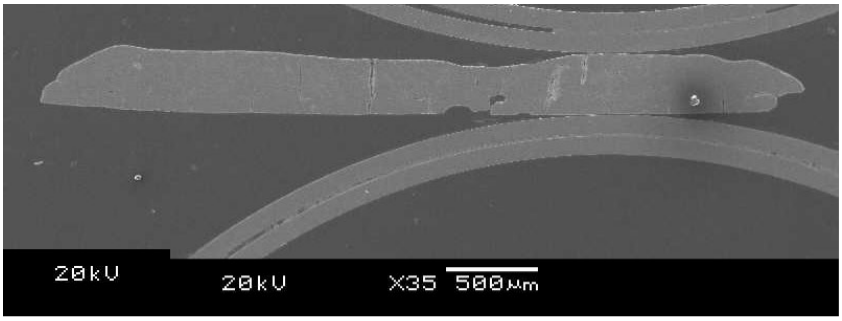

5-3-18 fired P8S3 left 35x.jpg

5-3-18 fired P8S3 right 35x.jpg

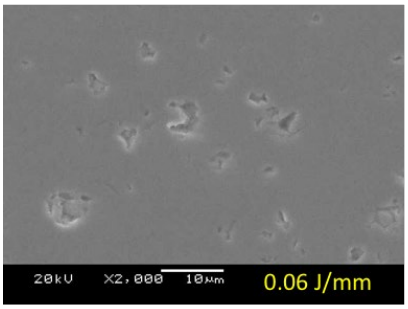

Laser power 18%. (6 Watts)
Raster speed 100 mm/sec, Field

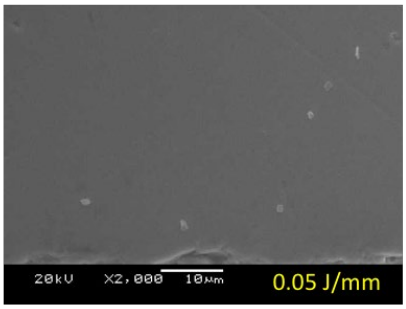

Laser power 20%. (10 Watts)
Raster speed 200 mm/sec, Field

Fig. 30 Polished cross section of three-layer part after furnace firing. Left and right side of the part have different lasing conditions. Porosity in photo at bottom left is a polishing artifact due to pull-out of ceramic grains during polishing.

8.4 Multilayer Parts: Ceramic Density after Furnace Firing

Three-layer ceramic squares were dispensed and lased with 8% YSZ slurry, a laser energy of 10 W, and a laser scan speed of 100 m/s. The parts were furnace-fired after selective laser sintering (SLS) process at various temperatures from 1250 °C to the recommended YSZ firing temperature of 1450 °C for 1 h. Ramp rate for the furnace was 5 °C/min ramping up to the firing temperature and 10 °C/min ramping down from the firing temperature. The samples were pyrolyzed in a tube furnace at 500 °C to remove organic material prior to the firing.

These samples were built on an alumina substrate to facilitate handling during the pyrolysis. The final density of the samples was measured with Archimedes method and is graphed in Fig. 31. Theoretical density of 8% YSZ according to the manufacturer Tosoh is 5.9 g/cc. The samples that were fired at 1450 °C measured 5.7 g/cc for the sample processed with an electric field and 5.1 g/cc for the sample processed without an electric field. Note the data outlier at 1350 °C. The data demonstrate that we are able to achieve 97% density with electric field after postprocessing.

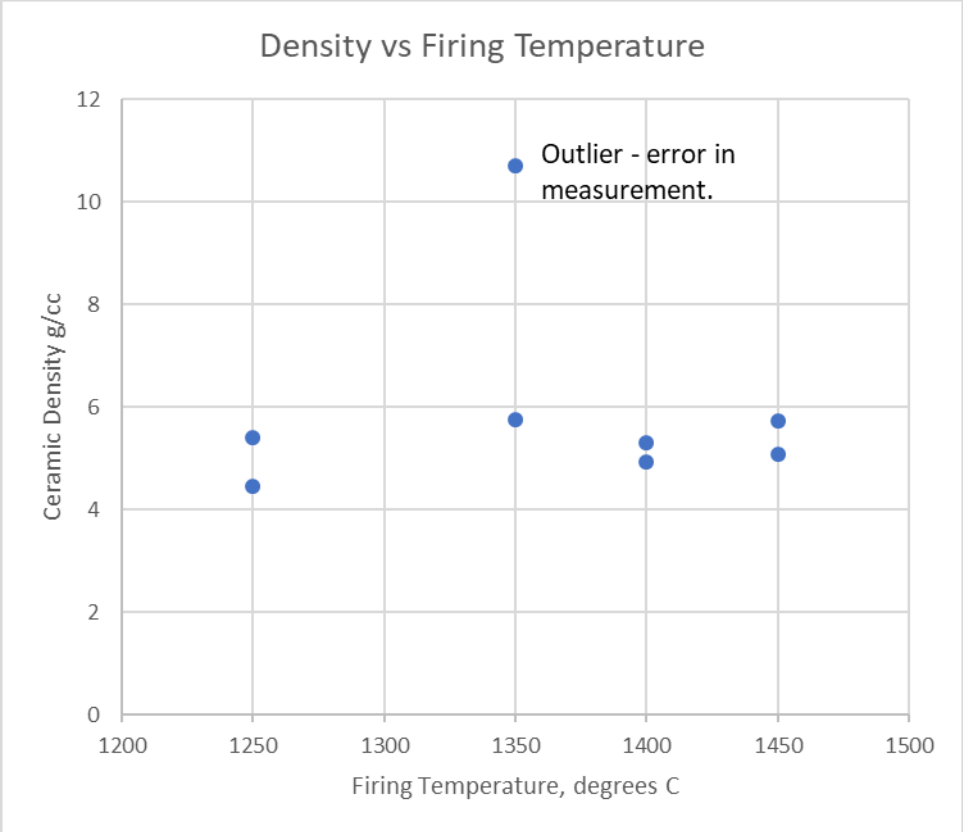

Fig. 31 Density vs. firing temperature; 8% YSZ ceramic multilayer n-Scrypt part

8.5 Raman Spectroscopy Data

Raman spectroscopy was done on ceramic samples scanned with various laser conditions to determine whether the beam was removing significant amounts of polymer from the slurry. Figure 32 shows top-down views of two parts after lasing. Only the highest-energy density samples showed any changes, and the ones with no visible changes are not shown.

Fig. 32 Samples 3 (left) and 10 (right) were lased with higher laser energy. Sample 3 shows a combination of removal of slurry from the base and blackened slurry. Sample 10 shows blackened slurry.

In Fig. 33, reference spectra are shown for the polymer without ceramic powder in the upper graph and the ceramic powder alone in the lower graph. Note the signature peak at approximately 2900 in the polymer scan. The peaks for the ceramic are in the region below 800.

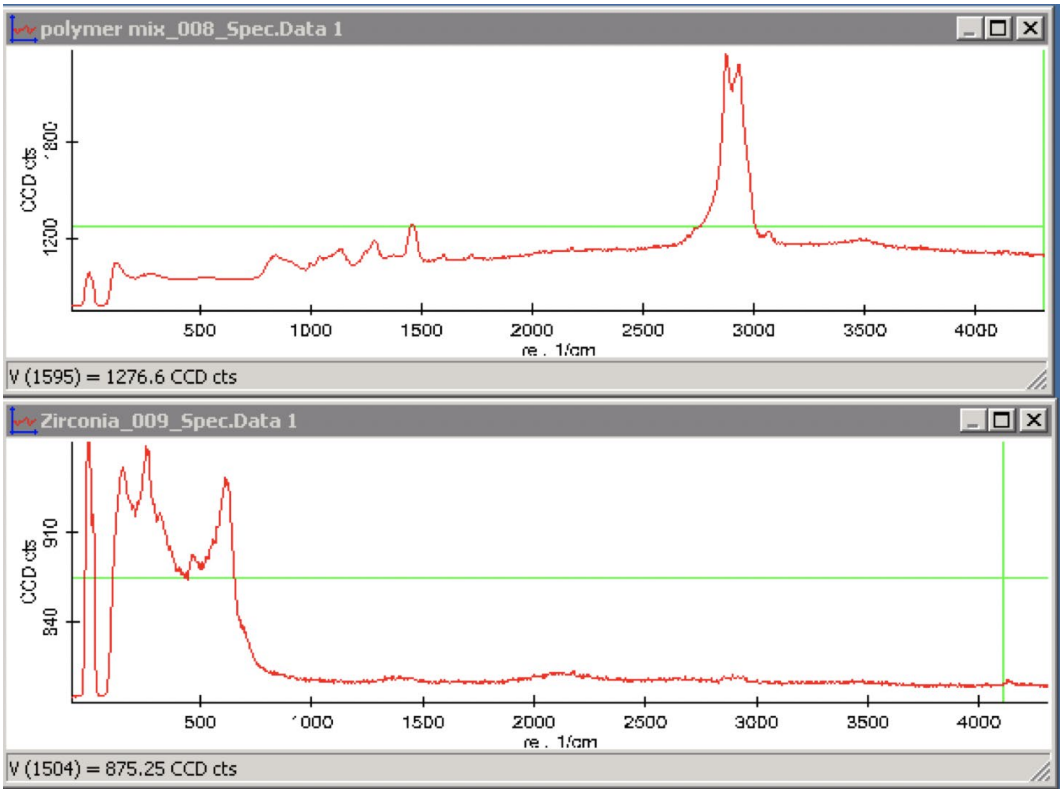

Fig. 33 (top) Reference spectra for the polymer without ceramic powder and (bottom) ceramic powder alone (bottom)

Comparing the reference spectra with the spectra of the lased parts, all spectra of parts that were not blackened after lasing showed significantly higher polymer peaks with respect to the ceramic peaks. Typical spectra of laser-scanned slurry are shown in Fig. 34. Note there is fluorescence in a broad energy zone centered at 2900. The signature peaks of the ceramic can be seen at 700 and below, and the signature polymer peak at 2900 is also visible. There were no significant differences between the scanned regions and the unscanned regions of the polymer except for parts that appear blackened. The blackened areas of the lased slurry had a Raman signature indicating elemental carbon, as shown in Fig. 35. The polymer in this area has been reduced to carbon. The peak at 2900 is not visible in the blackened areas, indicating that the polymer has been chemically altered.

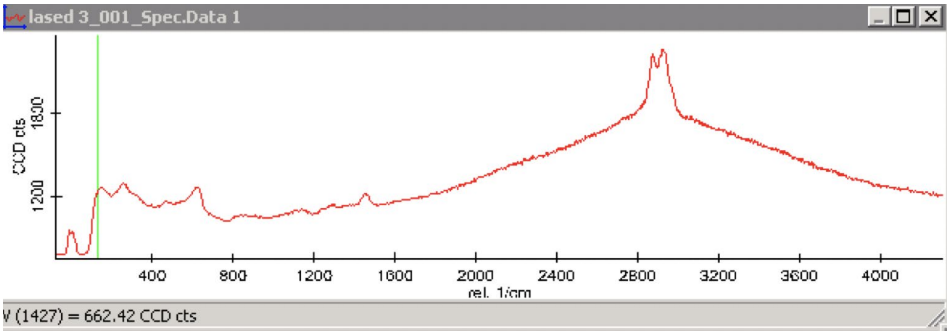

Fig. 34 Typical Raman spectroscopy results for a laser-scanned slurry. Laser scanned and unscanned regions of the nonblackened parts are very similar, meaning that in the nonblackened parts, most of the binder and plasticizer remain in the slurry after laser scanning.

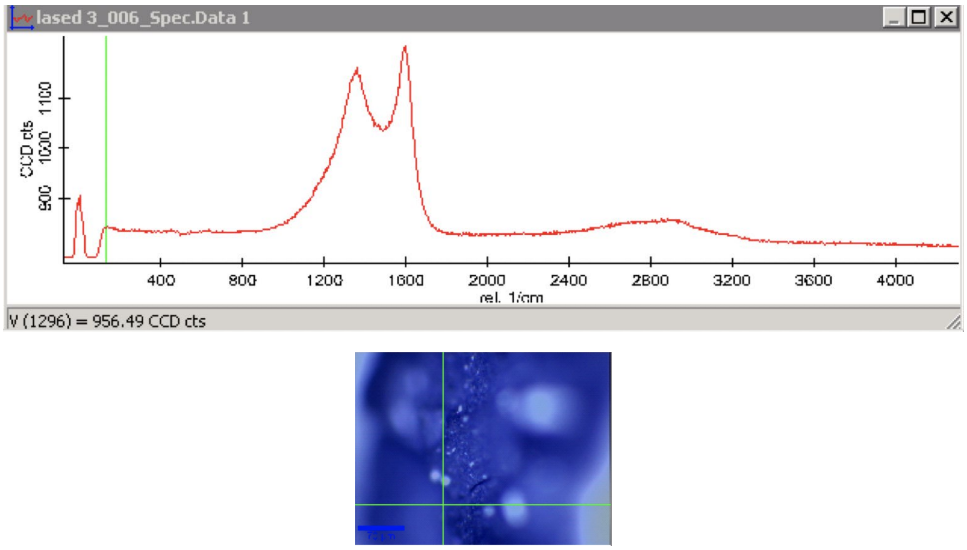

Fig. 35 (top) Raman of black areas in the scanned surface of Sample 3 shows a characteristic signature of elemental carbon, and (bottom) blackened area that was scanned

9. Conclusions and Recommendations

SLS processes use the energy of a laser to selectively fuse together powder particles, one layer at a time. The ceramic powder particles fuse directly together with ceramic necks between the particles. The polymer matrix is present to hold the powder in place and in a highly dense non-agglomerated packing structure until there is enough energy to fuse the ceramic together. It is instructive to examine in more detail the interaction of laser energy with the ceramic powder and the surrounding polymer matrix. Figure 36 illustrates the general interactions in a powder bed viewed as a cross section.

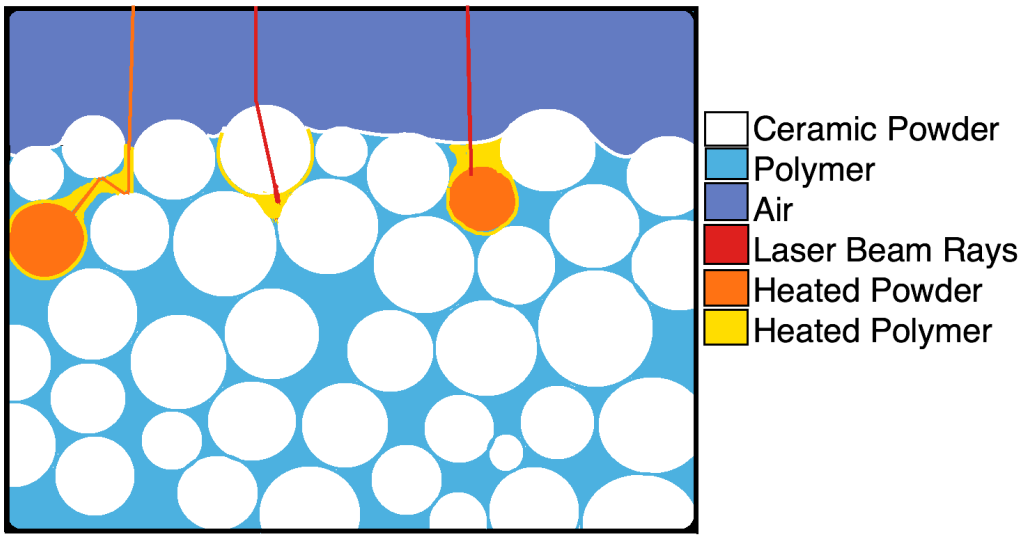

Fig. 36 Cross-section view of ceramic particles in slurry showing reflection, transmission, and absorption of laser energy (red lines)

Laser energy can be transmitted, absorbed, or scattered (reflected) by the polymer or the ceramic particles. The total energy is the sum of transmitted, absorbed, and reflected energy. Laser energy that is absorbed raises the temperature of the substance absorbing the energy. The amount of temperature rise depends on the absorptivity, the energy being absorbed, and the thermal properties of the material. Absorption, reflection, and transmission are material- and wavelength-dependent.

For direct laser sintering, it is desirable to have enough laser energy absorbed by the ceramic powder to enable rapid diffusion of the ceramic to form necks between ceramic particles. It is also desirable for the polymers to begin to break down and partially or completely pyrolyze during laser scanning of the layers as the necks are forming. However, if there is very low energy absorptivity of the ceramic powder, the temperature rise of the ceramic will be small. Ceramic necks form primarily with surface diffusion, whose rate is an exponential function of temperature. Low ceramic absorptivity leads to lower heat transfer, which results in lower ceramic temperature and corresponding slow diffusion rate of mass to form necks. Low ceramic absorptivity of the laser energy is therefore poor for direct sintering. Although we are supplementing the energy by application of an electric field, that addition of an electric field is not effective enough to counteract insufficient heating of the powder by the laser.

If the laser is absorbed by the polymer, the polymer temperature will rise. Although some of the heat will transfer from the polymer to the ceramic, the ceramic will remain at a lower temperature than the polymer. The polymers in the

slurry oxidize between 180 and 425 °C, which is insufficient for ceramic sintering. A large and rapid temperature rise in the polymer is likely to cause a rapid oxidation reaction. That rapid oxidation can take the form of a fire.

At powers below about 20% of maximum laser energy, Raman spectroscopy showed that the laser scan did not remove a significant amount of the polymer from the slurry. However, at greater than 20% maximum laser energy, there was a bright yellow light during lasing, as the polymers appeared to catch fire, leaving a black residue containing elemental carbon. This would happen if the oxidation reaction of air with polymer occurred rapidly, using up the oxygen locally and leaving a solid carbon residue rather than oxidizing into carbon dioxide or carbon monoxide gases. White zirconia powder was observed rising in eddy currents of hot gases from the flame. Without necks or polymer to hold the powder together, the ceramic powder was carried off along with the smoke from the fire. The white powder along with black soot also collected on the electrode surfaces when flame was seen.

In summary, the ceramic must absorb the laser energy to enable direct laser sintering, even if there is a large amount of scattering. Additionally, if pyrolysis of the polymer components of a slurry occurs before the ceramic powder heats sufficiently to form necks, the ceramic powder is likely to erode during the laser-induced pyrolysis.

10. Recommendations for Future Work

10.1 Ceramic Material, Laser, and Electric Field

It is recommended that direct sintering be done with a ceramic and laser combination that enables high absorption of the laser energy by the ceramic powder. All of the oxide materials are weak absorbers of 1-µm-wavelength laser energy. However, many carbides, such as SiC, absorb 1-µm-wavelength energy well. Switching the ceramic material to one that absorbs 1-µm wavelength is highly recommended for future evaluation of direct sintering in the n-Scrypt. Alternately, the laser can be replaced with one that has a wavelength that is easily absorbed by oxides, such as carbon dioxide lasers with a 10.6-µm wavelength.

Simulation of the electric field to understand the actual field at the sample will be very useful for understanding the science behind flash laser sintering processes of any material and equipment base. The actual field will vary with the height of the sample, layers beneath the electrode, dimensions of the part, applied voltage, dielectric constant, and the geometry of the electrodes. Simulation can help

determine which variables are significant and which are not, and will potentially help automate the process of establishing a uniform field over a variety of conditions.

10.2 Dispense of Slurry with n-Scrypt

The quality of parts made on the n-Scrypt is highly dependent on the slurry dispense quality. The rate of slurry dispense and therefore the volume of slurry dispensed per unit time will depend on several controllable variables, which include the following:

- Diameter of the pen tip opening
- Air pressure applied to the syringe plunger
- Rheology (e.g., viscosity) of the ink or slurry
- Amount and speed of the travel of the valve rod
- Speed of the x/y table (and therefore the rate of travel of the sample) under the pen tip
- Gap between the pen tip and the sample
- Wait times between opening of the valve rod and initiation of motion of the x/y table
- Surface tension of fluid, which depends on both the slurry or ink and the material type and surface finish of the sample

In addition, the following are uncontrolled process variables that significantly affect the dispense quality and dispense rate:

- Sticking of the plunger within the syringe
- Drying of the slurry or ink in the pen tip, resulting in partial or total obstruction of the pen tip opening
- Changes in viscosity due to shear rate of the slurry or ink as it flows through the pen tip
- Air bubbles in the slurry or ink

Sticking plungers, clogged pen tips, and shear-rate-dependent viscosities were major issues for print quality in the parts, causing uneven or blocked dispense, height and width variations across the dispense area, and unpredictable and highly irregular printing. The variations can be minimized by increasing the air pressure

to at least 70 psi, which helps with plunger sticking but does not eliminate it. Scrubbing the pen tip with a swab wetted with ethyl alcohol prior to dispensing helps to dissolve dried slurry or ink in the pen tip. The larger diameter pen tip opening also helps to reduce the amount of shear thinning behavior in the slurry because it reduces the shear rate of the material flowing through the nozzle. Ultimately, the process can be much better controlled by replacing the pneumatic system with a positive displacement mechanical pump, which is recommended in particular for multilayer parts.

These considerations affect any layer that is dispensed, but there are additional problems with dispense of multiple layers. Variation in dispensing volume results in height variations in the printed layer. Currently, there is significant variation in the dispensed height of the slurry. The pen tip cannot touch the layer beneath it, and if it does touch it will drag and destroy the lower layers. Therefore, the maximum height of existing layers defines the lowest height of the pen tip for a new layer. Tolerance stack-up of multiple layers will make it very difficult to make well-controlled parts in multiple layers. To mitigate this problem, extensive process development to limit the height variation is necessary. It will also be beneficial to use terrain-following sensing and software, which is available for n-Scrypt using laser distance scanning. However, it cannot be currently used in conjunction with a laser. This should be corrected by n-Scrypt with some modification of fixtures and software.

Using the heated stage will enable faster drying of layers and therefore faster production, and this can be investigated further. Retrofitting for controlled atmosphere will increase the breadth of materials that can be processed, particularly if laser sintering is used.

Additionally, the n-Scrypt software is not generally capable of making multilayer 3-D parts without extensive manual intervention, at least not in the dispense and lase area. The existing software is laborious for 3-D layers, but it does not have to be so.

Another improvement to the system is the alignment of the x/y stage with respect to the sample. Fiducials on the substrate would allow for automatic pattern recognition and feedback to an x/y position and theta rotation alignment schema. The current manual x/y homing and calibration technique is not adequate for a repeatable process. Automated z-height measurement is also recommended rather than manual z-homing of the pen tip.

There are some additional UT Austin resources in addition to the UT Additive Manufacturing Lab in The Center for Electromechanics that have extensive

expertise with these types of issues, including MERL (automation and integration of microelectronics for high precision and volume) and Dr Michael Cullinan's group at the University of Texas at Austin (micro SLS combined with dispensed metal inks).

10.3 Conclusions

This evaluation has demonstrated that multilayer ceramic parts can be made to full density using the n-Scrypt if a postprocessing furnace sintering is done. The n-Scrypt can make ceramic parts by using the dispense pattern to define the shape of the part successfully, which means that ceramic materials can be manufactured with the n-Scrypt slurry dispense system without a laser by doing an oven pyrolysis followed by a furnace firing of the dispensed multilayer shape. Software, process, and equipment development that focus on multilayer precision dispensing is recommended to enable high layer counts.

Laser flash sintering with oxide materials and YAG laser was not successful due to nonabsorption of the 1-µm-wavelength laser energy by the ceramic. With modification of the ceramic material to one that highly absorbs laser energy, along with a controlled atmosphere, the n-Scrypt can be used to develop laser flash sintered ceramic parts in the future. However, oxide materials in air atmosphere do not have the correct energy absorption profile at the 1-µm laser wavelength for enabling direct laser flash sintering. A change in the ceramic system to a carbide or nitride that absorbs 1-µm wavelength or a change in the laser wavelength will be required to further evaluate laser flash sintering on the n-Scrypt.

11. References

1. Naik KS, Dglavo VM, Raj R. Flash sintering as a nucleation phenomenon and a model thereof. Journal of the European Ceramic Society 2014;34(10):2435–2442.

2. National Fire Protection Association. The National Fire Protection Association 86 standard for ovens and furnaces, appendix D; 2015 [accessed 2018 Dec 10]. https://www.nfpa.org/codes-and-standards/all-codes-and-standards/list-of-codes-and-standards/detail?code=86.

List of Symbols, Abbreviations, and Acronyms

3-D	three-dimensional
AC	alternating current
alumina	aluminum oxide
AM	additive manufacturing
ARL	US Army Research Laboratory
DC	direct current
IR	infrared
MOR	modulus of rupture
R&D	research and development
SEM	scanning electron microscope
SLS	selective laser sintering
TGA	thermogravimetric analysis
UT Austin	University of Texas Austin
UV	ultraviolet
YAG	yttrium aluminum garnet
YSZ	yttria-stabilized zirconia
zirconia	zirconium dioxide

1 (PDF)	DEFENSE TECHNICAL INFORMATION CTR DTIC OCA
2 (PDF)	DIR CCDC ARL IMAL HRA RECORDS MGMT FCDD RLD CL TECH LIB
1 (PDF)	GOVT PRINTG OFC A MALHOTRA
1 (PDF)	CCDC ARL FCDD RLW MD M GAMMAGE